CHEMISTRY OF MATERIALS
Article

Chem. Mater. **2010,** *22,* 2937–2945 2937
DOI:10.1021/cm100255u

Calorimetric Measurement of Surface and Interface Enthalpies of Yttria-Stabilized Zirconia (YSZ)

Gustavo C. C. Costa,*,† Sergey V. Ushakov,† Ricardo H. R. Castro,†
Alexandra Navrotsky,† and Reginaldo Muccillo‡

†*Peter A. Rock Thermochemistry Laboratory and NEAT ORU, University of California at Davis, Davis, California 95616, and* ‡*Materials Science and Technology Center, Nuclear and Energy Research Institute, Sao Paulo, 05508-900 SP, Brazil*

Received January 27, 2010. Revised Manuscript Received March 4, 2010

The surface and interface enthalpies of cubic stabilized zirconia solid solutions containing 8, 10, and 12 mol % Y_2O_3 were determined by a combination of calorimetric, morphological, and structural analyses techniques. Nanocrystalline samples with several surface areas and degrees of agglomeration were synthesized by simultaneous precipitation and annealing at temperatures of 470−900 °C. Samples were characterized by X-ray diffraction and Raman spectroscopy. Surface areas were measured by N_2 adsorption, and interface areas were estimated by comparing surface areas from N_2 adsorption to those derived from an analysis of the crystallite sizes refined from X-ray diffraction data. Calorimetric measurements of heat of solution in a sodium molybdate melt, as a function of surface and interface areas, enabled us to experimentally derive trends in the surface and interface enthalpies of hydroxylated surfaces. Accounting for heats of water adsorption measured by microcalorimetry allowed us to obtain the surface enthalpies (energies) of the anhydrous surfaces at each composition. Average surface enthalpies were determined to increase with yttria content, from 0.85 ± 0.07 J/m^2 (for 8 mol % yttria) to 1.27 ± 0.08 J/m^2 (for 12 mol % yttria) for the hydrous surface and from 1.16 ± 0.08 J/m^2 to 1.80 ± 0.10 J/m^2 for the anhydrous surface. Interface enthalpies were determined to be in the range of 0.9 ± 0.5 J/m^2 for all studied compositions. Comparisons with measured surface energies for pure ZrO_2, and Y_2O_3 nanopowders and grain-boundary energies for YSZ dense nanoceramics are presented.

Introduction

There is increasing interest in both the scientific and industrial community in yttria-stabilized zirconia (YSZ)-based materials, because of their variety of applications in ceramics, solid oxide fuel cells, oxygen sensors, and catalysts.[1,2] Surface and interface energies in those materials are frequently referenced in discussions of processing and of other properties and phenomena; however, such energies are often considered difficult to derive using standard experimental techniques and no directly measured values for YSZ are available. Solution calorimetry has been exploited to measure surface enthalpies for pure ZrO_2,[3−5] Al_2O_3,[6,7] Fe_2O_3,[8,9] TiO_2,[10,11] and Y_2O_3,[12] and doped alumina compounds.[13] Because solids and liquids have small molar volumes and the pressure−volume (PV) term is small, the surface energy and surface enthalpy are essentially identical and can be used interchangeably.[14]

In this work, we present the results of surface energy measurements by high-temperature oxide melt solution calorimetry for hydrous and anhydrous cubic zirconia with 8, 10, and 12 mol % Y_2O_3. The samples were synthesized by simultaneous precipitation of cations and were annealed at different temperatures to produce a set of nanocrystalline powders with different surface areas. Structure, composition, and crystallite size were

*Author to whom correspondence should be addressed. Tel.: (530) 754-2133. Fax: (530) 752-9307. E-mail: gccosta@ucdavis.edu.

(1) Setter, N.; Waser, R. *Acta Mater.* **2000**, *48*(1), 151–178.
(2) Takahashi, T. *High Conductivity Solid Ionic Conductors*; World Scientific: Singapore, 1989; p 688.
(3) Radha, A. V.; Bomati-Miguel, O.; Ushakov, S. V.; Navrotsky, A.; Tartaj, P. *J. Am. Ceram. Soc.* **2009**, *92*(1), 133.
(4) Pitcher, M. W.; Ushakov, S. V.; Navrotsky, A.; Woodfield, B. F.; Li, G. S.; Boerio-Goates, J.; Tissue, B. M. *J. Am. Ceram. Soc.* **2005**, *88*(1), 160–167.
(5) Ushakov, S. V.; Navrotsky, A. Appl. Phys. Lett. **2005**, *87* (16), No. 164103.
(6) McHale, J. M.; Auroux, A.; Perrotta, A. J.; Navrotsky, A. *Science* **1997**, *277*(5327), 788–791.
(7) McHale, J. M.; Navrotsky, A.; Perrotta, A. J. *J. Phys. Chem. B* **1997**, *101*(4), 603–613.
(8) Mazeina, L.; Deore, S.; Navrotsky, A. *Chem. Mater.* **2006**, *18*(7), 1830–1838.
(9) Bomati-Miguel, O.; Mazeina, L.; Navrotsky, A.; Veintemillas-Verdaguer, S. *Chem. Mater.* **2008**, *20*(2), 591–598.
(10) Levchenko, A. A.; Yee, C. K.; Parikh, A. N.; Navrotsky, A. *Chem. Mater.* **2005**, *17*(22), 5428–5438.
(11) Ranade, M. R.; Navrotsky, A.; Zhang, H. Z.; Banfield, J. F.; Elder, S. H.; Zaban, A.; Borse, P. H.; Kulkarni, S. K.; Doran, G. S.; Whitfield, H. J. *Proc. Natl. Acad. Sci., U.S.A.* **2002**, *99*, 6476–6481.
(12) Zhang, P.; Navrotsky, A.; Guo, B.; Kennedy, I.; Clark, A. N.; Lesher, C.; Liu, Q. Y. *J. Phys. Chem. C* **2008**, *112*(4), 932–938.
(13) Castro, R. H. R.; Ushakov, S. V.; Gengembre, L.; Gouvea, D.; Navrotsky, A. *Chem. Mater.* **2006**, *18*, 1867–1872.
(14) Navrotsky, A. Thermochemistry of nanomaterials. In *Nanoparticles and the Environment*; Banfield, J. F., Navrotsky, A., Eds.; Reviews in Mineralogy & Geochemistry; Mineralogical Society of America: Chantilly, VA, 2001; Vol. *44*, pp 73−103.

Published on Web 03/24/2010

characterized using N_2 adsorption, X-ray diffraction (XRD), Raman spectroscopy, electron microscopy, and thermal analysis. Enthalpies for hydrous and anhydrous YSZ surfaces were determined on the basis of changes in measured solution enthalpy with surface and interface areas after correction for water adsorption enthalpy measured by microcalorimetry.

Comparison of total surface areas from N_2 adsorption with average crystallite size from XRD allowed delineation of the contribution of interface enthalpy to the total measured heat of drop solution. For the first time, we propose that solution calorimetry combined with structural and surface characterization techniques can be used to provide both surface and interface energies from a single set of samples. Experimentally measured values for surface energies are accurate enough to distinguish small differences between closely spaced compositions in the same structure type.

Experimental Section

Synthesis and Characterization. YSZ nanoparticles were synthesized using a simultaneous precipitation method. To obtain the initial stoichiometric solutions (0.5 mol/L), zirconium and yttrium nitrates ($ZrO(NO_3)_2 \cdot 2.4H_2O$ and $Y(NO_3)_3 \cdot 6H_2O$, respectively (99.9%, Alfa Aesar)) were dissolved into 30 mL of deionized water according to the molar ratios 5.75Zr:1Y (8 mol % Y_2O_3), 4.50Zr:1Y (10 mol % Y_2O_3) and 3.67Zr:1Y (12 mol % Y_2O_3). The stock solutions were added dropwise to 150 mL of 1 mol/L hydrazine hydrate $N_2H_4 \cdot H_2O$ (99%, Alfa Aesar) solution while stirring. The precipitates were centrifuged and washed with deionized water several times. They were dried in a vacuum oven at 200 °C overnight and then ground in an alumina mortar. After thermal characterization, the amorphous precipitates were annealed at 470−900 °C for 10 min to obtain samples with different surface areas.

The actual compositions of the synthesized samples were measured by wavelength-dispersive spectroscopy (WDS) electron probe microanalysis with a Cameca SX100 instrument at an accelerating voltage of 15 kV, beam current of 10 nA, and beam size of 1 μm. For microprobe analysis, powders were pelletized, sintered at 1500 °C, polished, and carbon-coated. This survived flat well-polished surfaces for analysis without changing the Y/Zr ratios. ZrO_2 and $Y_3Al_5O_{12}$ standards were used for Zr and Y. The sample compositions were calculated from an average of 10 data points.

Thermal analysis was performed using a Netzsch Model STA 449 system (Netzsch GmbH, Selb, Germany). Thermogravimetry (TG) and differential scanning calorimetry (DSC) traces were recorded upon heating 20−50 mg of samples in platinum crucibles at 20 °C/min in a 40 mL/min oxygen flow. Buoyancy corrections were made by recording baselines with empty crucibles for all runs. Evolved gases were analyzed using a Bruker Model Equinox 55 IR spectrometer (Bruker Optics, Inc.) (range of 400−4000 cm^{-1}) attached to the thermal analyzer by a transfer line heated at 150 °C. Crystallization enthalpy was obtained by integration of the exothermic peak using sensitivity calibration from heat capacity of a sapphire standard provided by Netzsch. Crystallization enthalpy values for every YSZ composition were calculated from an average of three experiments.

Powder XRD patterns were taken using a Bruker-AXS D8 Advance diffractometer (Bruker-AXS, Inc.) operated at an accelerating voltage of 40 kV and an emission current of 40 mA with Cu Kα radiation (λ = 0.15406 nm). Data were acquired over a range of 20°−100° 2θ with a step size of 0.02° and a collection time of 48 s/step. Crystallite sizes were refined from diffraction peak broadening, using a whole profile fitting procedure (Rietveld refinement), as implemented in the Jade 6.1 (MDI) software package.

Raman spectra were obtained at room temperature with a Raman Renishaw RM1000 system integrated with a Leica DMLM microscope with a motorized stage. Samples were excited with an Ar^+-ion laser (514.5 nm) operating at 9 A and 20 mW. Spectra were collected in a static range of 988−19 cm^{-1} with 10 accumulations of 60 s. A silicon film was used to calibrate the Raman shifts.

Transmission electron microscopy (TEM) was performed using a Phillips Model CM12 instrument operated at 120 kV with a LaB_6 filament. Samples were dispersed in methanol, ultrasonicated, and deposited on a lacey carbon grid. Magnification was calibrated using Ted Pella 603 latex spheres on a grating replica standard.

The surface areas were measured using a Micromeritics Model ASAP 2020 instrument, using the Brunauer−Emmett−Teller (BET) method. Five-point adsorption isotherms of the nitrogen were collected in the P/P^0 relative pressure range (where P^0 denotes the saturation pressure) of 0.05−0.3 at −196 °C. Prior to analysis, samples were degassed in a vacuum at 440 °C for 4 h.

Calorimetry. High-temperature oxide melt drop solution calorimetry was performed in a custom-made isoperibol Tian−Calvet twin microcalorimeter described by Navrotsky.[15,16] The calorimeter assembly was flushed with oxygen at 40 mL/min. Oxygen was bubbled through the solvent at 3 mL/min to aid dissolution. Five-milligram (nominal) pellets were loosely pressed, weighed, and dropped from room temperature into a $3Na_2O \cdot 4MoO_3$ solvent at 702 °C. Standard calibrations against the heat content of α-alumina were used. Prior to calorimetry, we equilibrated samples in the calorimetry suite for 72 h at 50% relative humidity. The water content of the samples (used in further calculations of enthalpy) was determined from weight loss on annealing at 1500 °C for 48 h; an average from five experiments was used for each sample.

Water adsorption enthalpy was measured at 25 °C using a combination of a Micromeritics Model ASAP2020 analyzer and a Setaram Model DSC111 Calvet microcalorimeter. The calorimeter was calibrated against the enthalpy of fusion of gallium metal. The instrumental design and measurement procedure were described earlier in detail.[5] Prior to water adsorption experiments, all samples were annealed at 800 °C in a vacuum of < 0.3 Pa. The total surface areas of the samples used for water adsorption were 7−10 m^2, and the vapor dose amount was calculated based on a total surface area of 1 μmol/m^2. One of the experiments with the 8YSZ sample was performed using a different setup with a factory-calibrated Setaram Sensys calorimeter and a Micromeritics Model ASAP2020 apparatus modified to allow gas manifold heating at 50 °C. All experiments were performed three times with degassing after the first adsorption sequence. The amount of water adsorbed on the empty tube was measured and used for correction of the total adsorbed amount in calculation of the integral enthalpy of adsorption.

(15) Navrotsky, A. *Phys. Chem. Miner.* **1977**, *2*(1−2), 89–104.
(16) Navrotsky, A. *Phys. Chem. Miner.* **1997**, *24*(3), 222–241.

Table 1. Summary of Data Used for Calculation of Surface and Interface Enthalpies for 8YSZ, 10YSZ, and 12YSZ Samples[a] (See Text for Details)

					H_2O (mol)		ΔH_{ds} for $3Na_2O \cdot 4MoO_3$ at 702 °C (kJ/mol)		
								YSZ[f]	
annealing temperature, T (°C)	BET SA ($\times 10^3$ m^2/mol)	cryst size XRD (nm)	XRD SA[b] ($\times 10^3$ m^2/mol)	IA[c]	z (total)[d]	c (chem.)[e]	YSZ·nH_2O[f]	hyd	anhyd
					12YSZ				
Bulk	0.07 ± 0.01						4.13 ± 0.59(5)		
900	2.9 ± 0.2	12.0 ± 0.3	7.9 ± 0.2	2.5 ± 0.2	0.068 ± 0.005	0.048 ± 0.005	3.05 ± 0.48(7)	−1.66 ± 0.54	−3.22 ± 0.68
800	5.1 ± 0.2	10.9 ± 0.3	10.3 ± 0.3	2.6 ± 0.1	0.153 ± 0.003	0.083 ± 0.005	6.92 ± 0.36(8)	−3.63 ± 0.39	−6.31 ± 0.64
750	6.2 ± 0.2	9.9 ± 0.3	11.4 ± 0.4	2.6 ± 0.1	0.209 ± 0.007	0.102 ± 0.007	9.50 ± 0.48(7)	−4.94 ± 0.61	−8.24 ± 0.91
700	9.7 ± 0.4	9.4 ± 0.2	12.5 ± 0.4	1.41 ± 0.08	0.258 ± 0.005	0.16 ± 0.01	9.67 ± 0.78(6)	−8.13 ± 0.82	−13.27 ± 1.27
					10YSZ				
Bulk	0.03 ± 0.02						4.17 ± 0.69(5)		
900	3.7 ± 0.1	14.4 ± 0.3	8.6 ± 0.2	2.5 ± 0.1	0.130 ± 0.004	0.049 ± 0.008	6.78 ± 0.21(6)	−2.17 ± 0.30	−3.89 ± 0.78
800	7.2 ± 0.3	11.4 ± 0.2	10.8 ± 0.2	1.82 ± 0.08	0.25 ± 0.01	0.97 ± 0.02	13.40 ± 1.97(5)	−4.11 ± 2.08	−7.49 ± 2.52
700	10.2 ± 0.3	9.8 ± 0.2	12.6 ± 0.3	1.20 ± 0.05	0.357 ± 0.004	0.14 ± 0.02	17.84 ± 0.49(8)	−6.81 ± 0.53	−11.61 ± 2.07
600	14.3 ± 0.3	8.6 ± 0.2	14.4 ± 0.4		0.538 ± 0.009	0.19 ± 0.03	26.40 ± 0.49(9)	−10.71 ± 0.66	−17.46 ± 2.86
					8YSZ				
Bulk	0.12 ± 0.04						4.83 ± 0.49(11)		
900	1.6 ± 0.4	19 ± 1	6.6 ± 0.2	2.5 ± 0.1	0.048 ± 0.005	0.016 ± 0.001	6.25 ± 1.24(7)	2.95 ± 1.27	2.45 ± 1.27
800	4.6 ± 0.4	15.0 ± 0.4	8.2 ± 0.3	1.8 ± 0.1	0.131 ± 0.003	0.048 ± 0.004	7.95 ± 0.37(6)	−1.11 ± 0.40	−2.56 ± 0.54
700	7.7 ± 0.3	12.9 ± 0.4	9.5 ± 0.3	0.88 ± 0.05	0.260 ± 0.009	0.080 ± 0.004	14.04 ± 1.08(7)	−3.92 ± 1.17	−6.35 ± 1.24
600	11.0 ± 0.4	12.1 ± 0.4	10.1 ± 0.4		0.382 ± 0.005	0.114 ± 0.006	21.74 ± 0.71(5)	−4.63 ± 0.76	−8.09 ± 0.96
470	12.4 ± 0.4	11 ± 1	10.8 ± 0.6		0.433 ± 0.002	0.129 ± 0.007	22.32 ± 2.44(10)	−4.57 ± 2.44	−8.48 ± 2.52

[a] Compositions from microprobe analysis are 8YSZ ($Zr_{0.86\pm0.01}Y_{0.14\pm0.01}O_{1.93\pm0.01}$), 10YSZ ($Zr_{0.83\pm0.01}Y_{0.18\pm0.01}O_{1.91\pm0.02}$), and 12YSZ ($Zr_{0.79\pm0.01}Y_{0.21\pm0.03}O_{1.90\pm0.01}$). [b] Calculated from crystallite size using theoretical densities of 5.959 g/cm^3 (8YSZ, PDF File Card No. 30-1468), 5.901 g/cm^3 (10YSZ, PDF File Card No. 81-1246), and 5.873 g/cm^3 (12YSZ, PDF File Card No. 77-2288). [c] IA = $^1/_2$(XRD SA − BET SA). [d] Measured by gravimetric analysis. [e] Calculated from adsorption data. [f] Values are means of the number of experiments given in parentheses; uncertainties are calculated as two standard deviations of the mean; extra digit is retained to prevent round-off error.

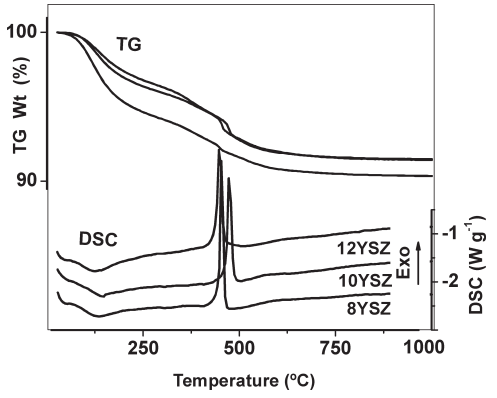

Figure 1. Thermogravimetry (TG) and differential scanning calorimetry (DSC) traces upon the heating of YSZ precipitates dried at 200 °C at a rate of 20 °C/min.

Results

Composition and Structure. Yttrium contents in synthesized $Zr_{1-x}Y_xO_{2-(x/2)}$ measured by electron microprobe were close to nominal stoichiometries: 0.14 for 8YSZ, 0.18 for 10YSZ, and 0.21 for 12YSZ (see Table 1). The analyzed compositions were used in the thermochemical calculations. Figure 1 shows TG and DSC traces for the as-precipitated samples dried at 200 °C. Upon heating to 300 °C, the samples underwent a weight loss of 4%−6% with a corresponding endothermic effect. Evolved gas analysis (Fourier transform infrared analysis, FTIR) revealed only water vapor. Crystallization of YSZ occurred at 400−500 °C, as evident from the exothermic peak on the DSC trace. This effect is accompanied by a steep weight loss of ∼4 wt %, which is also attributed to residual water after gas analysis. No significant weight loss was observed above 750 °C. Crystallization was confirmed by XRD patterns of samples treated at temperatures higher than the temperature of the exothermic crystallization peak (470−900 °C), as shown in Figure 2 for the three compositions. In all cases, there is no evidence for yttria or monoclinic zirconia phases. Because of the broad diffraction peaks, one could not distinguish whether the crystallized nanophase YSZ is cubic or tetragonal.

The studied compositions lie within the stability range of the cubic phase at the synthesis temperatures.[17] However, it is common to obtain tetragonal YSZ as a second phase during crystallization if the yttrium distribution in the precipitate is not homogeneous. The adopted synthesis procedure was designed to avoid the formation of traces of tetragonal phase. That is, by adding Zr and Y nitrate solutions into a hydrazine excess, one minimizes possible local variations in the yttrium concentration caused by solubility differences between yttrium and zirconium hydroxides. Raman analysis confirmed the absence of the tetragonal phase in our samples. The spectrum in Figure 3 for 10YSZ clearly exhibits only one band, at 619 cm^{-1}, which is characteristic of the cubic fluorite structure, whereas tetragonal zirconia is expected

(17) Chevalier, J.; Gremillard, L.; Virkar, A. V.; Clarke, D. R. *J. Am. Ceram. Soc.* **2009**, *92*(9), 1901–1920.

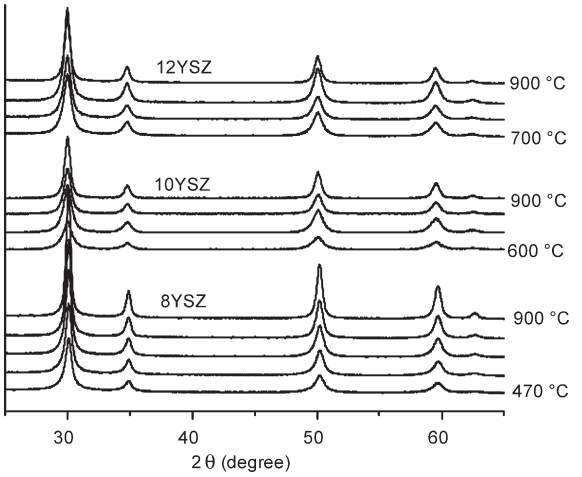

Figure 2. XRD patterns of nanocrystalline YSZ powders used for calorimetry (see Table 1). Samples synthesized by annealing precipitates at temperatures of 470−900 °C for 10 min. Crystallite size was refined from peak broadening using whole profile fitting.

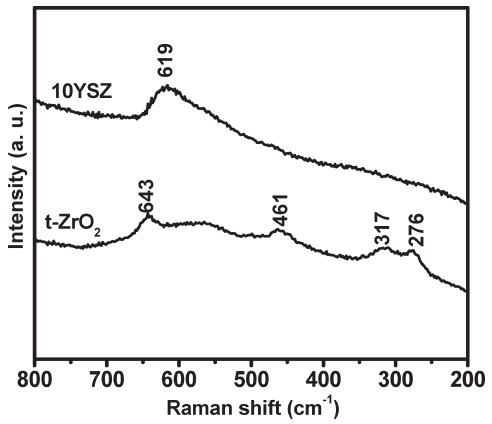

Figure 3. Raman spectrum of nanocrystalline cubic yttria-stabilized zirconia (10YSZ in Table 2). A Raman spectrum of nanocrystalline tetragonal zirconia (t-ZrO_2) used in a previous study,[4] taken under similar conditions, is shown for comparison.

to have six Raman-active modes (shown in Figure 3 for reference).[18−21]

Revisiting Figure 2, we may now attribute all diffraction peaks to the cubic fluorite (*Fm*3*m*) structure and determine the crystallite sizes after whole pattern fitting refinement. Table 1 shows crystallite sizes for the three compositions heat-treated at different temperatures. An increase in the crystallite size with annealing temperature is observed for all samples, reflecting coarsening or grain growth. The lattice parameters for YSZ samples with different crystallite size were determined to be within experimental error for a given composition and increase linearly with yttria content. The average values of the lattice parameters are 0.51347(3) nm for 8YSZ, 0.51451(5) nm

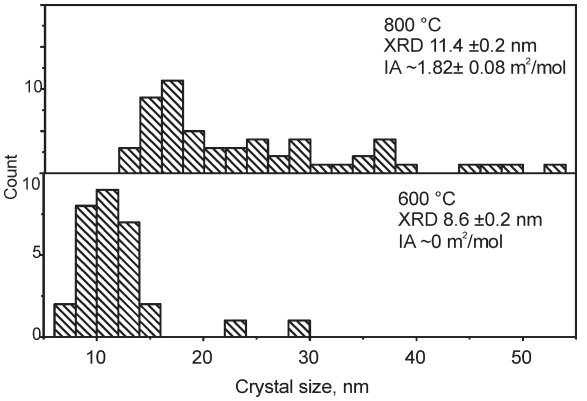

Figure 4. Size distributions in 10YSZ powders from measurement of 30−50 crystals in TEM. Powders were synthesized by annealing of precipitate at 600 and 800 °C. The average crystal size refined from XRD peak broadening and IA, calculated as (XRD SA − BET SA)/2, is shown for comparison.

for 10YSZ, and 0.51493(4) nm for 12YSZ, consistent with earlier reports.[22]

Crystal Sizes, Surface, and Interface Areas. Upon increasing the annealing temperature from 600 °C to 900 °C, the surface area of YSZ decreased from ~14 m^2/mol to ~4 m^2/mol, as determined by the BET method from N_2 adsorption (see Table 1). N_2 adsorption detects only solid/vapor interfaces and any interface area (solid/solid, IA) is not included in the BET area values. Peak broadening in XRD patterns, on the other hand, is sensitive to crystallite size, rather than overall particle size. Assuming spherical crystallites (which is reasonable in this case, because of the relatively isotropic nanoparticles), it is possible to calculate the "XRD surface area" (XRD SA) from crystallite size, refined from the broadening of peaks in XRD patterns and reference values for the densities, and from TEM measured sizes. For nonagglomerated fully crystalline powders, XRD SA and TEM SA must be consistent with BET SA (because there would be no nonaccessible interfaces). If the surface area from BET measurement is much higher than that calculated from XRD crystallite sizes, the presence of amorphous material is likely. If the surface area from BET measurements is substantially lower than that calculated from XRD crystallite sizes, the existence of IA can be inferred and their areas estimated.

Table 1 shows that BET and XRD SA are reasonably close only for the sample annealed at 600 °C, when the average crystallite size of 8.6 nm translates to an XRD SA value of ~14.4 m^2/mol, which is essentially the same as the BET SA value (14.3 m^2/mol). Similar correspondences of BET SA and XRD SA are observed for 8YSZ and 12YSZ samples annealed below 700 °C. For samples annealed above 700 °C, the crystallite size from XRD translates to surface areas substantially larger than those from BET. TEM analysis of 10YSZ detects agglomerated nanocrystalline powders, confirming

(18) Feinberg, A.; Perry, C. H. *J. Phys. Chem. Solids* **1981**, *42*(6), 513–518.
(19) Ishigame, M.; Sakurai, T. *J. Am. Ceram. Soc.* **1977**, *60*(7−8), 367–369.
(20) You, J. L.; Jiang, G. C.; Xu, K. D. *Chin. Phys. Lett.* **2001**, *18*(3), 408–410.
(21) Kourouklis, G. A.; Liarokapis, E. *J. Am. Ceram. Soc.* **1991**, *74*(3), 520–523.
(22) Ioffe, A. I.; Rutman, D. S.; Karpachov, S. V. *Electrochim. Acta* **1978**, *23*(2), 141–142.

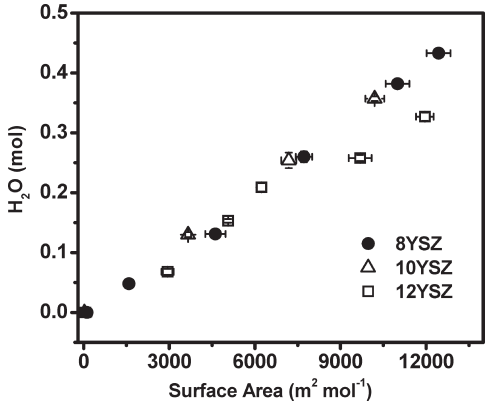

Figure 5. Total water content of YSZ samples used for drop solution calorimetry from gravimetric analysis.

substantial IA for higher temperatures of annealing (700 and 800 °C) and not as much for the lower temperature (600 °C), as shown in the size distribution in Figure 4. For 10YSZ samples annealed at 600, 700, and 800 °C, average particle sizes from TEM were determined as 12 ± 2, 17 ± 2, and 24 ± 3 nm, respectively, from measurements of 30−50 particles. These values are consistent with XRD sizes, because they reflect polycrystalline nanoparticles rather than single crystals, considering the quantitative limitations of the TEM used.

Because, during the aggregation of the powders, the interface is formed by two surfaces, the interface area (IA) can be calculated as follows:

$$\mathrm{IA} = \frac{(\mathrm{XRD\ SA}) - (\mathrm{BET\ SA})}{2}$$

Meaningful values for interface areas are calculated for samples annealed at 700 °C and above. In powders annealed at 900 °C, the total interface area is approximately the same as the surface area accessible for N_2 adsorption (BET SA) (Table 1). Solution calorimetry data for nonaggregated and aggregated YSZ powders allows calculations of both surface and interface enthalpies, as described below.

Drop Solution and Water Adsorption Calorimetry. The enthalpies of drop solution for YSZ·nH$_2$O are summarized in Table 1, together with water contents of the samples (see Figure 5). Two values for water content are given, per mole of YSZ. The first (z total) corresponds to the total water content in the nanocrystalline powder samples as measured by prolonged annealing at 1500 °C and weighing the coarsened samples. The term "c(chem)" represents the amount of water with enthalpy of adsorption more negative than −44 kJ/mol (this is the enthalpy of condensation of water vapor), calculated from the BET surface area of samples and chemisorbed coverage determined by water adsorption calorimetry (see Table 2). Chemisorbed coverage increases from ~6 H_2O nm^{-2} to 11 H_2O nm^{-2} as the yttria content increases from 8 mol % to 12 mol %. For all studied compositions, the integrated enthalpy of adsorption of chemisorbed water is in the range of −76 ± 5 kJ/mol (see Table 2), with no meaningful variation with composition.

Table 2. Experimental Details and Integral Adsorption Enthalpies for Water Vapor on the Surface of Cubic Stabilized Zirconia Annealed at 850 °C

	Value		
parameter	8YSZ	10YSZ	12YSZ
surface area (m^2/g)	59.4 ± 0.7	61.4 ± 0.4	80.5 ± 0.7
sample mass (mg)	150.2	114.9	133.9
coverage for the 1st dose (H_2O nm^{-2})	0.7 ± 0.1	0.59 ± 0.04	0.54 ± 0.04
$-\Delta H_{ads}$ (kJ/mol)	123 ± 10	133 ± 4	132 ± 12
~50% chemisorbed coverage (H_2O nm^{-2})	3.2 ± 0.2	4.3 ± 0.6	4.9 ± 0.3
$-\Delta H_{ads}$ (kJ mol^{-1})	93 ± 5	96 ± 2	96 ± 4
chemisorbed coverage (H_2O nm^{-2})	6.3 ± 0.3	8 ± 1	11 ± 1
$-\Delta H_{ads}$ (kJ/mol)	74 ± 2	79 ± 3	78 ± 4

Measured drop solution enthalpies of YSZ·nH$_2$O were corrected for water content, considering the thermochemical cycle below and assuming that water in the sample is energetically equivalent to liquid water (taking c = 0 in the cycle below, ΔH_5 = YSZ "hydrous"), or by taking the enthalpy of desorption to be the negative of measured adsorption enthalpy (c values from Table 1, ΔH_5 = YSZ "anhydrous").

$$\mathrm{Zr}_{1-x}\mathrm{Y}_x\mathrm{O}_{2-(x/2)}z\mathrm{H_2O}_{(\mathrm{surface,298\,K})} \rightarrow \mathrm{Zr}_{1-x}\mathrm{Y}_x\mathrm{O}_{2-(x/2)(\mathrm{sln,975\,K,\,975K})} + z\mathrm{H_2O}_{(\mathrm{g,975\,K,\,975K})}$$
$$\Delta H_1 = \Delta H_{ds}$$

$$z\mathrm{H_2O}_{(\mathrm{g,975\,K})} \rightarrow z\mathrm{H_2O}_{(\mathrm{g,298\,K})}$$
$$\Delta H_2 = z(-25.0 \pm 0.1)\ \mathrm{kJ/mol}$$

$$(z-c)\mathrm{H_2O}_{(\mathrm{g,\,298K})} \rightarrow (z-c)\mathrm{H_2O}_{(\mathrm{surface,\,298K})}$$
$$\Delta H_3 = (z-c)(-44.0 \pm 0.1)\ \mathrm{kJ/mol}$$

$$c\mathrm{H_2O}_{(\mathrm{g,298\,K})} \rightarrow c\mathrm{H_2O}_{(\mathrm{surface,298\,K})}$$
$$\Delta H_4\ (\mathrm{kJ/mol}) = c(-\Delta H_{ads})$$

$$\mathrm{Zr}_{1-x}\mathrm{Y}_x\mathrm{O}_{2-(x/2)(\mathrm{nano,298\,K})} \rightarrow \mathrm{Zr}_{1-x}\mathrm{Y}_x\mathrm{O}_{2-(x/2)(\mathrm{sln,975\,K})}$$
$$\Delta H_5 = \Delta H_{\mathrm{corr\,ds(nano)}}$$

$$\Delta H_5 = \Delta H_1 + \Delta H_2 + \Delta H_3 + \Delta H_4$$

where ΔH_1 is the measured drop solution enthalpy, and ΔH_4 is the measured adsorption enthalpy. ΔH_2 and ΔH_3 are reference values.[23] As shown previously,[3,5,12] this data

(23) Robie, R. A.; Hemingway, B. S. *Thermodynamic Properties of Minerals and Related Substances at 298.15 K and 1 bar (10(5) pascals) Pressure and at Higher Temperatures*; U.S. Geological Survey Bulletin 2131; U.S. Geological Survey: Reston, VA, 1995.

Table 3. Calculations of Surface Energy (SE) and Interface Enthalpy (IE) Values from Drop Solution Enthalpies (See Text for Details)

sample	hydrous SE (J/m^2)[a,b]	hydrous IE (J/m^2)[a,b]	anhydrous SE (J/m^2)[a,b]	anhydrous IE (J/m^2)[a,b]
		All Samples Using BET SA (1)		
12YSZ	1.46 ± 0.05 (5)		2.00 ± 0.07 (5)	
10YSZ	1.16 ± 0.03 (5)		1.72 ± 0.11 (5)	
8YSZ	1.02 ± 0.05 (6)		1.32 ± 0.06 (6)	
		Samples with BET SA ~ XRD for SE (2)		
12YSZ	1.27 ± 0.08 (2)	0.60 ± 0.15 (4)	1.80 ± 0.13 (2)	0.63 ± 0.22 (4)
10YSZ	1.04 ± 0.05 (2)	0.99 ± 0.15 (4)	1.51 ± 0.20 (2)	0.97 ± 0.41 (4)
8YSZ	0.85 ± 0.07 (3)	0.91 ± 0.28 (4)	1.16 ± 0.08 (3)	0.82 ± 0.32 (4)
		All Samples Using Multiple Linear Regression (3)		
12YSZ	1.11 ± 0.11 (5)	0.87 ± 0.24 (5)	1.63 ± 0.16 (5)	0.92 ± 0.35 (5)
10YSZ	1.00 ± 0.04 (5)	1.05 ± 0.14 (5)	1.46 ± 0.15 (5)	1.08 ± 0.41 (5)
8YSZ	0.89 ± 0.06 (6)	0.92 ± 0.25 (6)	1.21 ± 0.07 (6)	0.83 ± 0.31 (6)

[a] Numbers in parentheses correspond to number of samples used for calculations. [b] Extra digit retained to avoid round-off error.

treatment allows one to calculate the enthalpies of both hydrous and anhydrous surfaces.

Discussion

Crystallization Enthalpies of YSZ. Crystallization enthalpies, determined from integration of the exothermic peaks, were −13.7 ± 0.6 kJ/mol for 8YSZ, −12.7 ± 0.2 kJ/mol for 10YSZ, and −11.7 ± 0.5 kJ/mol for 12YSZ. They decrease in magnitude by 2 kJ/mol when the yttrium content increases from $x = 0.14$ (8YSZ) to 0.21 (12YSZ), although this small change is barely outside experimental error. As previously reported,[24] cubic compositions with $x = 0.09$ and 0.33, synthesized by precipitation from chloride solution with ammonium hydroxide, crystallize in the range 411−435 °C, with crystallization enthalpies of −19 and −12 kJ/mol. Despite the differences in synthesis routes, the values for crystallization enthalpies are in general agreement. The crystallization enthalpy found in this work for 8YSZ is also in good agreement with the value reported by Ramanathan et al.[25] Similar surface areas of the studied compositions after crystallization indicates that change in crystallization enthalpy with yttrium content is not related to the contribution of surface energy but reflects differences in the energetics of the bulk material. Because H_2O is evolved during crystallization, the energetics of that (endothermic) process will also contribute to the observed crystallization enthalpy. Thus, the enthalpy of crystallization may be more exothermic for hypothetical anhydrous nanoparticles.

Water Adsorption Enthalpies. The integral enthalpies of chemisorbed water are between −75 kJ/mol and −80 kJ/mol, with no obvious dependence on yttria content, but the coverage increases with yttria content from 6 H_2O nm^{-2} to 11 H_2O nm^{-2}. After Brunauer,[26] the dissociative adsorption monolayer coverage can be taken as ~4−5 H_2O nm^{-2} and, for molecular adsorption, as 8−10 H_2O nm^{-2}. Thus, the increase in coverage may be indicative of some shift from dissociative to molecular adsorption with increasing yttria content. However, any such change does not appear to leave a signature in the energetics.

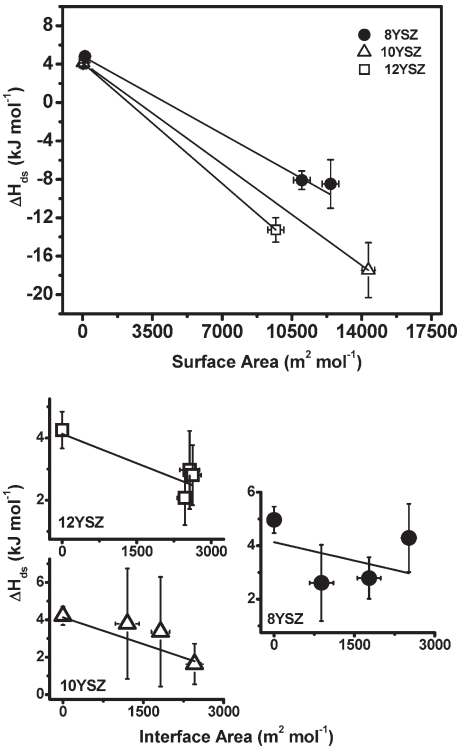

Figure 6. Drop solution enthalpies of nanocrystalline cubic zirconia samples with 8, 10, and 12 mol % yttria versus BET surface area (top) and interface area (bottom). The negative of slopes of the linear fit corresponds to surface and interfacial energies.

Surface and Interface Energies Calculations. We tested three approaches for calculating the surface and interfacial enthalpies from solution calorimetry data (Table 1). The results are shown in Table 3.

In the first case, drop solution enthalpies for all samples of given composition were fitted as linear function of BET surface area (see Figure 6):

$$\Delta H_{ds}(\text{nano}) = \Delta H_{ds}(\text{bulk}) - \text{SE}(\text{BET SA}) \qquad \text{(all samples)} \tag{1}$$

This approach was used for preliminary analysis of first calorimetry data on YSZ.[27] It inherently overestimates

(24) Ushakov, S. V.; Brown, C. E.; Navrotsky, A. *J. Mater. Res.* **2004**, *19*(3), 693–696.
(25) Ramanathan, S.; Muraleedharan, R. V.; Roy, S. K.; Nayar, P. K. K. *J. Am. Ceram. Soc.* **1995**, *78*(2), 429–432.
(26) Brunauer, S.; Kantro, D. L.; Weise, C. H. *Can. J. Chem.* **1956**, *34*, 1483–96.

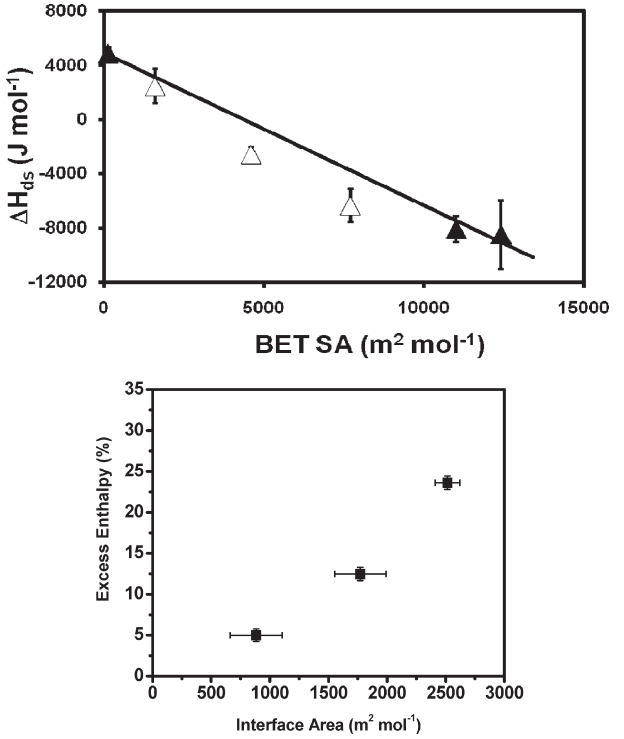

Figure 7. (Top) Drop solution enthalpies of all 8YSZ samples vs BET surface area; open symbols represent samples with significant interface area. The exothermic deviation from drop solution enthalpy trend from nonaggregated samples is evident. (Bottom) Percentage of the excess enthalpy related to the interface versus interface area for anhydrous 8YSZ.

surface energy (SE) by considering both surface and interfacial enthalpy as a function of surface area alone. We also note that the fit of all the data at a given composition to a straight line is not very good and some curvature is suggested (see Figure 7).

In the second case, only samples for which no significant aggregation was detected (e.g., BET SA = XRD SA, IA = 0) were used for calculations of surface energies:

$$\Delta H_{ds}(\text{nano}) = \Delta H_{ds}(\text{bulk}) - \text{SE(BET SA)} \quad (\text{samples with IA} = 0) \qquad (2a)$$

The obtained values of surface energies can then be used to calculate interfacial energies (IE) from the samples with detectable interface area:

$$\Delta H_{ds}(\text{nano}) = \Delta H_{ds}(\text{bulk}) - \text{SE(BET SA)} - \text{IE(IA)} \quad (\text{using SE from eq 2a}) \qquad (2b)$$

This approach uses only two or three data points to derive surface energy. In Figure 7, drop solution enthalpies for 8YSZ are plotted versus BET surface area. Only solid symbols are used to calculate the slope of the function; open symbols are used to derive the interfacial energy.

In the third case, all data are used simultaneously to derive both surface and interfacial enthalpy, using a multiple linear regression fit:

$$\Delta H_{ds} = \Delta H_{ds}(\text{bulk}) - \text{SE(BET SA)} - \text{IE(IA)} \quad (\text{all samples}) \qquad (3)$$

This approach was originally proposed by one of the co-authors[28] to process calorimetry datasets for samples with varying surface/interface areas. In our case, it includes data points with nonzero interfacial area into refinement of surface energy values. This approach would be the only way to treat data where some interfacial area is detected in all samples.

Linear regressions fits were performed using Origin 8.0 software, using propagated uncertainties in drop solution values to weigh data during fitting. Surface and interfacial enthalpies calculated from cases 2 and 3 are essentially within calculated uncertainties. Because some samples in our datasets exhibit no aggregation, we choose the surface energies values calculated using the second approach to be the most reliable, because it is difficult to estimate accuracy in XRD surface areas.

Using drop solution enthalpies corrected for chemisorbed water (ΔH_{ds} YSZ "anhyd" in Table 1), we obtained energies for anhydrous surfaces: 1.16 ± 0.08, 1.51 ± 0.20, and 1.80 ± 0.13 J/m^2 for 8YSZ, 10YSZ, and 12YSZ, respectively. Using drop solution enthalpies corrected considering all water physisorbed (ΔH_{ds} YSZ "hydrous" in Table 1), we obtain values for hydrous surfaces: 0.85 ± 0.07, 1.04 ± 0.05, and 1.27 ± 0.08 J/m^2 for 8YSZ, 10YSZ, and 12YSZ, respectively. Interfacial enthalpy is the same for the hydrous and anhydrous case (0.9 ± 0.5 J/m^2), and its variation with YSZ compositions is within experimental uncertainty.

Comparison with Previous Experimental and Theoretical Studies. In studying the energy crossovers among polymorphs in pure nanocrystalline zirconia experiments performed earlier in our laboratory,[4] we found that the surface area obtained from XRD is higher than that obtained from BET for all crystalline samples of monoclinic and tetragonal zirconia. In that work, a Micromeritics Model Gemini 2360 instrument was used for surface area measurement, which did not allow evacuation below 5 Pa. The degassing of the samples prior to BET analysis was performed at 5 Pa and room temperature. In the follow-up water adsorption study on tetragonal zirconia,[5] we remeasured BET surface area for one of the tetragonal sample using a Micromeritics Model ASAP 2020 instrument with turbomolecular pump and sample degas at 800 °C, and found agreement of BET and XRD surface area, which indicated nonagglomerated powder. The average values for hydrous and anhydrous surface enthalpies of tetragonal zirconia were derived as 1.02 ± 0.05 and 1.23 ± 0.04 J/m^2. However, later studies on nanopowders of monoclinic zirconia with degassing at high temperature under vacuum[3] corroborated the earlier established difference in surface area from XRD crystallite size and BET surface area, indicating heavy twinning and/or aggregation.

(27) Costa, G. C. C.; Ushakov, S. V.; Navrotsky, A.; Muccillo, R. *Mater. Res. Soc. Symp. Proc.* **2009**, 1122E.

(28) Castro, R. H. R. Unpublished work, **2009**.

Table 4. Summary of Data Used To Calculate Enthalpies of Drop Solution of the Samples Involved in the Thermochemical Cycle To Obtain the Enthalpy of Formation of Nanocrystalline Cubic $Zr_{1-x}Y_xO_{2-(x/2)}$[a]

		γ (J/m^2)					$\Delta H_{f,ox}$ (kJ/mol)	
	SA (m^2/mol)	hyd	anhyd	$\Delta H_{ds(bulk)}$ (kJ/mol)	$\Delta H_{ds(hyd)}$ (kJ/mol)	$\Delta H_{ds(anhyd)}$ (kJ/mol)	hyd	anhyd
$Y_2O_{3(cubic)}$[b]	6774	1.25 ± 0.17	1.66 ± 0.14	−60.5 ± 2.2	−68.97 ± 2.22	−71.75 ± 2.20		
$ZrO_{2(mono)}$[c]	3217	2.86 ± 0.31	3.45 ± 0.28	19.5 ± 0.9	8.93 ± 0.95	6.75 ± 0.94		
8YSZ	3654	0.85 ± 0.07	1.16 ± 0.08	4.83 ± 0.49	1.72 ± 0.49	0.59 ± 0.50	−3.69 ± 1.03	−4.82 ± 1.02
10YSZ	3643	1.04 ± 0.05	1.51 ± 0.20	4.17 ± 0.69	0.37 ± 0.69	−1.35 ± 0.72	−5.03 ± 1.25	−5.61 ± 1.27
12YSZ	3592	1.27 ± 0.08	1.80 ± 0.13	4.13 ± 0.59	−0.49 ± 0.60	−2.42 ± 0.60	−6.93 ± 2.33	−7.31 ± 2.40

[a] Extra digit is retained to prevent round-off error. [b] See ref 12. [c] See ref 3.

The YSZ surface energies reported here are similar to values for pure tetragonal zirconia. Thus, there does not seem to be a strong driving force from surface energy to stabilize the cubic form, relative to the tetragonal form at the nanoscale. This suggests that the stabilization of cubic YSZ at both bulk and nanoscales is largely a function of its bulk chemistry.

A recent work by Xia et al.[29] reported calculated surface energies for YSZ with 8% Y_2O_3. Their value for the most stable relaxed (111) surface (1.2 J/m^2) is the same as the surface enthalpy for anhydrous 8YSZ obtained experimentally in this work.

The value of 0.7 ± 0.2 J/m^2 for the grain-boundary energy of $Y_{0.16}Zr_{0.84}O_{1.92}$ previously determined[30] by solution calorimetry of nanopowders densified using spark plasma sintering into ceramics with negligible surface area but large interfacial area is consistent with our findings despite possible difference in the interfaces and surface areas measurements methods. The values for surface enthalpy are reported in the same paper as 1.6 and 2.2 J/m^2 for hydrous and anhydrous nanoparticle surfaces. They are somewhat higher than our results for a similar composition. However, the earlier values were based on a single-nanocrystalline sample, and the possibility of an interfacial enthalpy contribution was not considered.

Enthalpies of Formation for Nanosized YSZ vs Bulk YSZ. Table 4 shows the calorimetric data needed to calculate the enthalpies of formation ($\Delta H_{f,ox}$) of nano *c*-YSZ at 25 °C for both hydrous and anhydrous surfaces of the nanopowders. The enthalpy of drop solution measured for samples of coarse cubic-stabilized zirconia—4.83 ± 0.48 kJ/mol for 8YSZ, 4.17 ± 0.69 kJ/mol for 10YSZ, and 4.13 ± 0.59 kJ/mol for 12YSZ—are within the uncertainty of the previously measured value (3.50 ± 0.96 kJ/mol) reported[31] for $Zr_{0.8}Y_{0.2}O_{1.9}$. Enthalpies of drop solution of nanocrystalline samples of monoclinic zirconia ($ZrO_{2,mon}$), cubic yttria ($Y_2O_{3,cubic}$), and YSZ were calculated using the linear equation

$$\Delta H_{ds(nano)} = \Delta H_{ds(bulk)} - \gamma SA$$

where $\Delta H_{ds(nano)}$ and $\Delta H_{ds(bulk)}$ are the drop solution enthalpies (kJ/mol) of the nanoparticles and the bulk, respectively, γ is the surface enthalpy of a particular zirconia polymorph, and SA is the surface area (SA = 30 m^2/g).

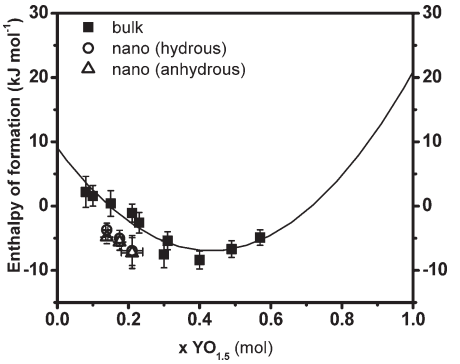

Figure 8. Enthalpy of formation for nanocrystalline and bulk[31] cubic $Zr_{1-x}Y_xO_{2-(x/2)}$ versus yttrium content.

The enthalpies of formation of nanocrystalline cubic YSZ at 25 °C, with respect to nanocrystalline oxides $ZrO_{2(mono)}$ and $Y_2O_{3(cubic)}$, $\Delta H_{f,ox}$ (nano c-YSZ), are derived from a thermodynamic cycle as following and the values are presented in Table 4 and Figure 8.

$$Zr_{1-x}Y_xO_{2-(x/2)(c\text{-}YSZ,298\,K)} \rightarrow Zr_{1-x}Y_xO_{2-(x/2)(sln,975\,K)}$$
$$\Delta H_1 = -\Delta H_{ds(c\text{-}YSZ)}$$

$$ZrO_{2(monoclinic,298\,K)} \rightarrow ZrO_{2(sln,975\,K)}$$
$$\Delta H_2 = (1-x)\Delta H_{ds(ZrO_2(mono))}$$

$$YO_{1.5(cubic,298\,K)} \rightarrow YO_{1.5(sln,975\,K)}$$
$$\Delta H_3 = x\Delta H_{ds(Y_2O_3(cubic))}$$

$$ZrO_{2(monoclinic,298\,K)} + YO_{1.5(cubic,298\,K)} \rightarrow Zr_{1-x}Y_xO_{2-(x/2)(c\text{-}YSZ,298\,K)} \qquad \Delta H_4 = \Delta H_{f,\,ox(nano\ c\text{-}YSZ)}$$

$$\Delta H_4 = \Delta H_1 + \Delta H_2 + \Delta H_3$$

where x and $1 - x$ are the yttrium and zirconium contents in the sample, respectively, as determined by microprobe analysis. ΔH_2 and ΔH_3 are reference values.[3,12] For illustrative purposes, the calculations were done for particle sizes of 40 nm for $Y_2O_{3(cubic)}$ and 34 nm for $ZrO_{2(mon)}$ and YSZ (surface areas of 30 m^2/g). The particle sizes were calculated using the theoretical densities 5.034 g/cm^3

(29) Xia, X.; Oldman, R.; Catlow, R. *Chem. Mater.* **2009**, *21*(15), 3576–3585.
(30) Chen, S. S.; Avila-Paredes, H. J.; Kim, S.; Zhao, J. F.; Munir, Z. A.; Navrotsky, A. *Phys. Chem. Chem. Phys.* **2009**, *11*(17), 3039–3042.
(31) Lee, T. A.; Navrotsky, A.; Molodetsky, I. *J. Mater. Res.* **2003**, *18* (4), 908–918.

($Y_2O_{3(cubic)}$, PDF Card No. 64-8262) and 5.823 g/cm^3 ($ZrO_{2(mon)}$, PDF Card No. 64-5482), and the densities of YSZ from the footnote in Table 1.

The mixing behavior of nano c-YSZ follows the same trend as that observed by Lee et al.[31]for bulk material. However, the enthalpies of formation for nano c-YSZ are slightly more negative than those for bulk YSZ. This is attributed to the additional contribution of the high surface enthalpy of nanocrystalline monoclinic ZrO_2, which results in less endothermic enthalpies of drop solution (ΔH_{ds}) in the thermochemical cycle.

Conclusion

Surface and interface energies were derived for three compositions of YSZ using drop solution calorimetry, accompanied by microstructure analysis. We showed that both surface and interface energies can be derived from the same set of solution calorimetry data. The recommended values of surface energies for anhydrous surfaces of cubic YSZ powders obtained in this work are 1.16 ± 0.08 J/m^2 for 8YSZ, 1.51 ± 0.20 J/m^2 for 10YSZ, and 1.80 ± 0.13 J/m^2 for 12YSZ. The interface energies for all studied compositions are within 0.9 ± 0.5 J/m^2. Disregarding the contribution of interfacial energies in interpretation of solution calorimetry data for aggregated nanopowders generally leads to an overestimation of surface energies.

Acknowledgment. This work was supported by the U.S. Department of Energy (Grant No. DE-FG02-03ER46053). G.C.'s work at the Peter A. Rock Thermochemistry Laboratory was partially funded by the International Institute for Complex Adaptive Matter (NSF Grant No. DMR0645461). We express deep appreciation for the valuable discussions and help from Tatiana Shvareva, and we thank James Hughes for comments on the manuscript. R.C. thanks UC Davis for startup funds.